

# Optimization of FSW Processing Factors on Hardness for Dissimilar AA6061-T6 and AZ31B O Alloys

Karutha Pandian Vasantha Kumar\* – Muthusamy Balasubramanian  
Anna University, University College of Engineering Ramanathapuram, India

*In modern industries, such as aerospace, automotive, marine and others, aluminium and magnesium alloys are the most frequently used non-ferrous materials. This paper discusses optimising processing factors to produce a high hardness of dissimilar Al/Mg alloys. The experiment was designed and conducted by varying input factors according to response surface methodology-central composite design. The regression model has been developed between the processing factor and hardness based on the results of the experiment. ANOVA is used to validate the regression model and to assess the percentage of each hardness factor's contribution. Finally, the desirability approach is used to optimise the processing factor for high hardness.*

**Keywords:** dissimilar friction stir welding, aluminium alloy AA6061, magnesium alloys AZ31B, FSW, RSM, ANOVA

## Highlights

- Tool rotation and traverse speeds were important factors in determining the Vicker's hardness of the FSW welded Al/Mg alloy.
- High rotational speed and low transverse speed resulted in high hardness at the weld area.
- Rotational speed, traverse speed, and tilt angle have 28.24 %, 42.72 %, and 19.70 % influence on hardness, respectively.
- Traverse speed has a higher influence than other factors, such as rotational speed and tilt angle.
- The maximum Vicker's hardness value at the weld zone achieved by the experiment is 92 HV.
- The optimal setting for achieving high hardness (i.e., 92 HV) is at  $S = 1000$  rpm,  $T = 30$  mm/min and  $A = 2$  deg at a desirability value of 0.98.
- The results of the confirmatory test show that hardness of FSWed Al/Mg Alloys is 92.5 HV and tensile strength is 182 MPa.
- The hardness of dissimilar FSWAl/Mg alloy is 92 HV, which is 85 % of the hardness of Al alloy and 110 % of hardness of Mg alloy.

## 0 INTRODUCTION

Friction stir welding is advantageous for non-ferrous alloys, such as Al and Mg. Aluminium alloy 6061 offers various advantages, such as a high strength-mass ratio, excellent welding, and excellent corrosive endurance. Due to its high specific solidity and lower density, the use of magnesium AZ31B alloys in different industries has increased. However, existing methods for welding Al and Mg alloys have several disadvantages. Joining aluminium and magnesium alloys with FSW eliminates the majority of the difficulties associated with the current procedures.

Fig.1a shows FSW, a solid-state welding procedure that uses frictional heat generated by a rotating tool to weld materials. Weld quality in FSW is determined by process factors, tool design, and material properties of both the welding material and the tool [1] to [3]. Compared to the leaving side, high hardness in the weld zone is on the progressing side. Furthermore, in the welding of aluminium alloys, the traverse speed is the most important factor [4].

The profile of a tool probe and the ratio of a pin to shoulder diameter are the most crucial tool design factors in determining weld quality [5]. Malarvizhi

et al. [6] examined the impact of the diameter of the tool shoulder on the tensile, macrostructural, and microstructural characteristics of the Mg and Al alloys. Welding circumstances that lead to an adequate intermingling among different materials and the intermediary thermal input have been useful in attaining high-level weld attributes [7]. Verma et.al.[8] concluded that low rotational speed and high transverse speed resulted in poor hardness because there was insufficient time and frictional heat to form an atomic bond between the Al and Mg alloys.

Li et al. [9] investigated the effects of rotation and traverse speed on the mechanical and microstructure characteristics of the AZ31B-Magnesium alloy, concluding that high weld quality can be achieved with moderate heat input. A fine microstructure is observed in the weld zone, according to Singh et al. [10], indicating an increase in hardness in a welded joint. According to Devaiah et al. [11], tool rotation speed and traverse speeds were important factors in determining the mechanical properties of the FSW-welded Al alloy. Increased rotational speed or decreased traverse speed on FSW joints resulted in high hardness in the stir zone [10] and [13]. A suitable tool offset can improve joint quality by preventing defects, such as voids and tunnels,

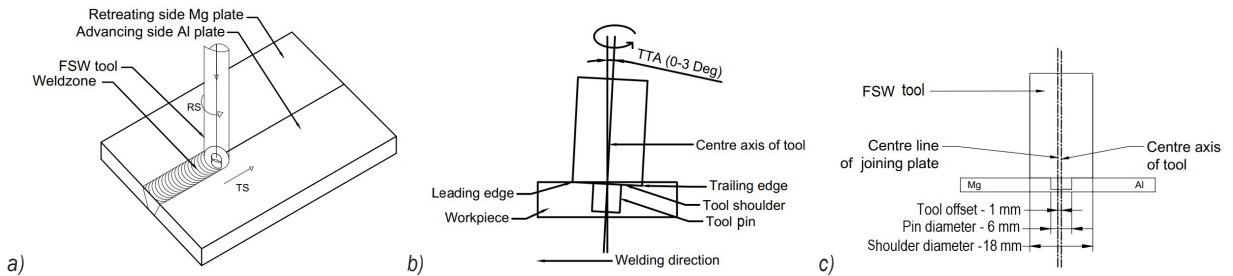


Fig. 1. a) FSW process, b) tool tilt angle, and c) tool offset

and reducing intermetallic compounds thickness to improve the interface bonding strength of the dissimilar weld during the friction stir welding (FSW) processes [14]. The response surface methodology (RSM) is a statistical technique for optimising multi-parameter and response optimization. RSM is widely used because of its simplicity and flexibility, as well as the ease with which individual factors and responses can be identified [15] and [16]. Most researchers concentrate solely on the tensile strength of welded material. The microstructures of welded aluminium and magnesium alloys have been analysed by various researchers [17] to [19].

In this paper, the effect of processing factors on the hardness of dissimilar FSW of Al/Mg alloys is analysed in depth. The Al alloy (AA6061-T6) and Mg alloy (AZ31B) are friction stir-welded in this research to evaluate the change in hardness at various process factors. The experiment architecture is developed using the RSM-central composite designed (CCD) technique by changing the process factor. The impact of each factor on the hardness of the FSW Al-Mg alloy has been investigated, and the desirability approach was used to optimise the process factor to achieve a high hardness of welded joints.

## 1 EXPERIMENTAL DETAILS

The FSW experiments were performed with the AA6061 aluminium alloy and the AZ31B magnesium alloy. The chemical components of welding plates are shown in Table 1. The surface of the aluminium and magnesium plate was cleaned with acetone, and the oxide on the surface was removed with a steel wire brush. The plate's dimensions are 75 mm × 50 mm × 4 mm. The tool pin profile and the ratio of shoulder and pin diameter are important design parameters in determining weld quality in the FSW procedure [5]. The FSW welding of Al and Mg plates were performed with a cylindrical pin profiled WC tool. Fig. 1c illustrates the FSW tool specification.  $D_s/D_p$

= 3 (shoulder to pin diameter ratio) are constant. On the advancing side, the rotational tool was inserted at a 1 mm offset from the joining baseline, as shown in Fig. 1c. The diameter of the shoulder and pin of the tool are 18 mm and 6 mm, respectively, and the length of the probe is 3.8 mm. By varying processing factors, the experiments are designed using RSM – CCD techniques.

Table 1. Chemical composition of workpieces

Workpieces	AA6061-T6	AZ31B-O
Al	Balance	2.06
Mn	0.5	0.31
Zn	0.006	0.84
Fe	0.4	0.018
Cu	0.24	0.002
Cr	0.209	-
Si	0.67	<0.001
Ni	0.02	-
Mg	0.97	Balance
Vicker's Hardness		
Vickers hardness	107 HV	83 HV

### 1.1 Identification of Processing Parameter

The primary processing factors are the tilt angle, traverse speed, axial force, and rotation speed. The processing factors and their range are shown in Table 2. The hardness of the weld is entirely determined by the amount of heat applied via various factors. Thermal input has a direct relationship with axial force and rotation speed. If the traverse speed is low, the friction between tool and workpiece is high, which increases the temperature at the nugget zone and vice versa. Eq. (1) expresses the relationship between the processing factor and the heat input.

$$Q_{Input} = \frac{2\pi}{3T} \times \mu \times F \times S \times R_s \times \eta, \quad (1)$$

whereas  $T$  is traverse speed,  $S$  is rotation speed,  $F$  is an axial force,  $R_s$  is a radius of the shoulder,  $\eta$  is efficiency, and  $\mu$  is coefficient of friction.

**Table 2.** Processing factor and their range

S. No.	Processing factor	Ranges
1	Rotation speed ( $S$ )	600 rpm to 1000 rpm
2	Traverse speed ( $T$ )	30 mm/min to 60 mm/min
3	Tool tilt angle ( $A$ )	0 deg to 2 deg

RSM-CCD techniques are used in this experiment to examine the impact of processing variable that influences the hardness at the welded zone. The RSM with desirability approach is employed to predict the best processing factors to achieve high hardness in welded areas. Tool tilt angle, traverse speed, and rotation speed all directly impact the hardness of FSW joints, which can be expressed in Eq. (2).

$$Y = f(S, T, A). \tag{2}$$

This equation provides a mathematical model that shows how the joint hardness is related to the processing factor. In the select processing factor ranges given in Table 3, this model is developed to analyse the hardness of the welded joints.

**Table 3.** Variation level of processing factor

Processing factor	Levels		
	-1	0	1
$S$ [rpm]	600	800	1000
$T$ [mm/min]	30	45	60
$A$ [deg]	0	1	2

## 2 RESULTS AND DISCUSSION

### 2.1 Results of Hardness Test

The fracture or crack occurs at the welded zone in the low hardness regions. In this present study, hardness evaluation near welded areas and processing factor optimization achieve better results. FSW experiments with multiple combinations of processing factors are performed. The specimen is prepared according to standards for the Vicker’s hardness test are shown in Fig. 2. The hardness test carried out using Vicker’s hardness tester in the weld area is shown in Fig. 3. Table 4 shows the hardness of the joints using Vicker’s hardness testing under load.

The mathematical relationship is generated on the basis of the results to detect the effect of each factor

and their interaction on the hardness of the welded joint. Eq. (3) expresses the regression equation for the hardness of welded joint.

$$\begin{aligned}
 HV = & 118.5 - 0.1011 \times S - 0.34 \times T + 7.24 \times A \\
 & + 0.000068 \times S \times S - 0.00101 \times T \times T \\
 & - 1.177 \times A \times A + 0.000221 \times S \times T \\
 & + 0.00294 \times S \times A - 0.0842 \times T \times A. \tag{3}
 \end{aligned}$$

**Table 4.** Experimental Results of hardness test

S. No.	$S$ [rpm]	$T$ [mm/min]	$A$ [deg]	Hardness [HV]
1	600	30	2	83
2	600	60	0	66
3	600	30	0	75.6
4	600	60	2	70.3
5	600	45	1	74.4
6	800	30	1	81.5
7	800	45	1	76.2
8	800	45	1	77
9	800	45	1	75.9
10	800	45	1	78.3
11	800	45	1	74.6
12	800	45	0	71.6
13	800	60	1	70
14	800	45	2	78
15	800	45	1	78
16	1000	45	1	83
17	1000	30	0	80.3
18	1000	60	2	80
19	1000	30	2	92
20	1000	60	0	75.3

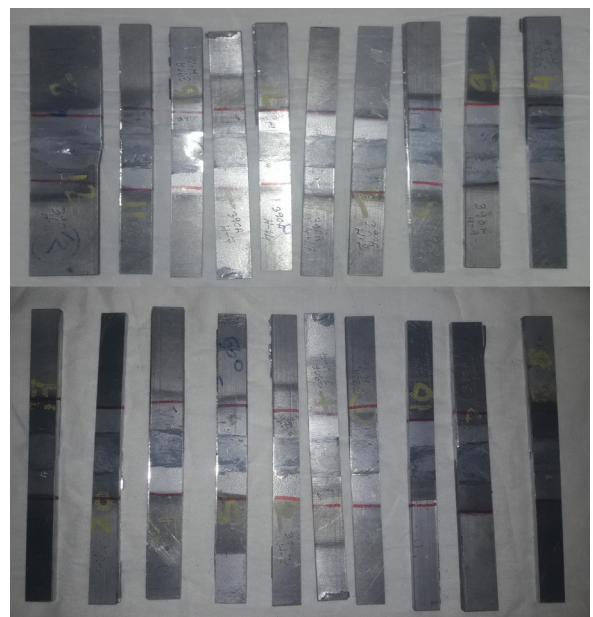


**Fig. 2.** Specimen after hardness test

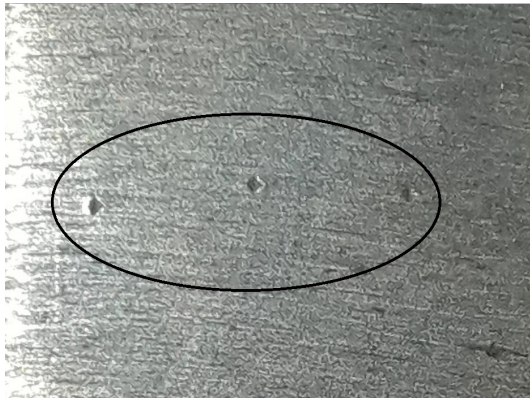


Fig. 3. Hardness test carried out in the weld zone

## 2.2 ANOVA Analysis

The effectiveness of the mathematical model is tested with ANOVA. The impact of each factor (rotational speed (RS), traverse speed (TS) and tool tilt angle (TTA)) on the response (hardness) is also determined [15] and [20]. The ANOVA table generated based on the experiment result with the help of Minitab software is represented in Table 5. To identify the contributions of each factor on response was evaluated using Eq. (4).

$$\%C = \frac{\sum SS_{Individual}}{\sum SS_{Total}} \times 100, \quad (4)$$

where  $C$  is the percentage contributed by the individual factor,  $SS_{Individual}$  the sum of square contributed by

the individual factor, and  $SS_{Total}$  the total of “sum of square” contributed by all factors. The  $F$ -value model of 45.32 implies that the model is meaningful. Very few chances of error in the  $f$  value due to noise.  $P$ -value lesser than 0.05 indicates that the terms in the model are significant. The  $F$ -value and  $P$ -values model, therefore, prove that the model is adequate and effective.

The model’s fitness is based on the  $R^2$  determination coefficient. Table 6 shows the corresponding statistical values for the developed model. The signal-to-noise ratio is sufficiently accurate. It is desirable to have a ratio above 4. The ANOVA results indicate that its result is valid. The percentages contribution from rotational speed, traverse speed and tilt angle are 28.24 %, 42.72 % and 19.70 %, respectively.

The residual analysis was performed to check the model’s accuracy. The graphical method of checking that errors commonly occur in distribution is the normal probability plots [21]. Fig. 4 shows the normal probability plot. The residuals almost follow a straight line, which shows that the error follows the normal distribution.

The residual vs fitted chart is a scatter plot of residues on the  $y$ -axis and an estimated response is to detect the random distribution of residues on the  $x$ -axis and the constant variation of residues [22]. Fig. 5 shows the residual vs fitted value plot, the residues on both sides of the middle line are equally distributed.

Table 5. ANOVA table

Source	DF	SeqSS	AdjMS	%C	F-value	P-value
Model	9	589.60	65.51	97.61%	45.32	<0.001
Linear	3	547.66	182.55	90.66%	126.30	<0.001
$S$	1	170.57	170.57	28.24%	118.01	<0.001
$T$	1	258.06	258.06	42.72%	178.55	<0.001
$A$	1	119.03	119.03	19.70%	82.35	<0.001
Square	3	22.92	7.64	3.79%	5.28	0.02
$S \times S$	1	17.67	20.39	2.93%	14.10	0.00
$T \times T$	1	1.43	0.14	0.24%	0.10	0.76
$A \times A$	1	3.81	3.81	0.63%	2.64	0.14
2-Way Interaction	3	19.02	6.34	3.15%	4.39	0.03
$S \times T$	1	3.51	3.51	0.58%	2.43	0.15
$S \times A$	1	2.76	2.76	0.46%	1.91	0.20
$T \times A$	1	12.75	12.75	2.11%	8.82	0.01
Error	10	14.45	1.45	2.39%		
Lack-of-Fit	5	4.82	0.96	0.80%	0.50	0.77
Pure-Error	5	9.63	1.93	1.59%		
Total	19	604.05		100.00%		

From the residual analysis, the generated mathematical models are accurate, and they can be utilized to forecast the hardness of a welded joint within a given range of processing factors.

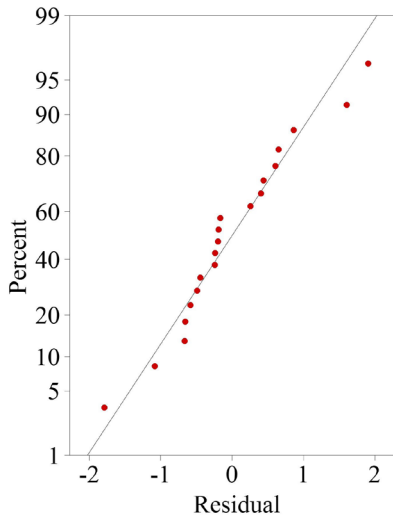


Fig. 4. Normal probability plot

Table 6. Fit statistics

$R^2$	$R^2(\text{adj})$	$R^2(\text{pred})$
97.61 %	95.45 %	87.77 %

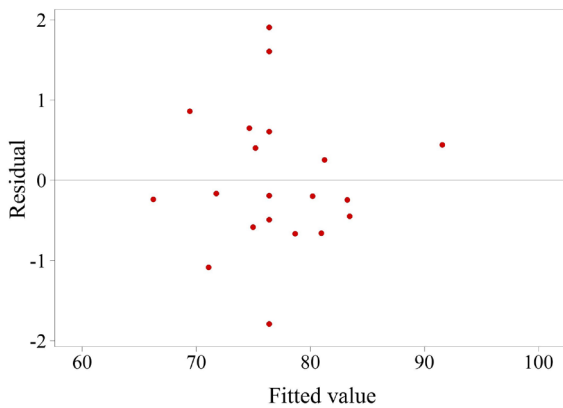


Fig. 5. Residual vs. fitted value plot

### 3 EFFECT OF FSW PARAMETER ON HARDNESS:

#### 3.1 Effect of the Individual Parameter

The mean effect plots show that joint hardness is increased at a high tilt angle, high rotation, and low traversing speed at the welded region. When rotating speed and tilt angles are increased, the hardness at the welded zone improves. When the traverse speed

is reduced, the joint hardness in the welded zone is increased. The primary cause of the hardness changes is the heat input. The mean effect plot has been created using Minitab software, which shows the change of hardness for input factors such as  $RS$ ,  $TS$  and  $TTA$  is shown in Fig. 7. According to the ANOVA results, rotation speed, traverse speed, and tilt angle all contribute 28.24 %, 42.72 %, and 19.70%, respectively. Fig. 6. shows a pie chart that was created based on the ANOVA results. It shows that the traverse speed has a greater influence on the tool tilt angle than the rotation speed.

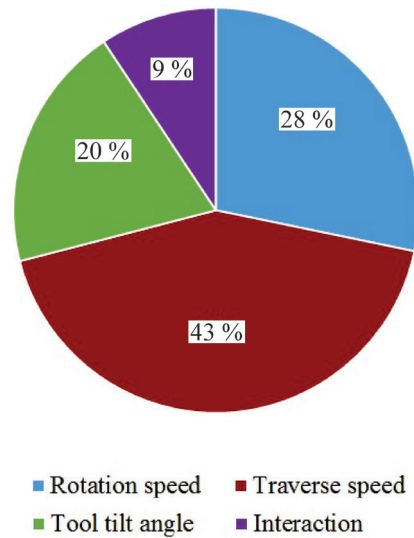


Fig. 6. Influence of each factor on the hardness

#### 3.2 Effect of the Interaction Parameter

The traverse speed and tool tilt angle have high influences in a two-way interaction, as shown by interaction plots (Fig. 8). An interaction plot is created using Minitab software that shows the hardness variation in the interaction between processing factors. Compared to individual processing factors, the contribution of squared and interaction of processing factors is less in the ANOVA table. On hardness, the combined percentage contribution of squared and interaction processing factors is 9 %. The pareto chart depicts the graphical representation of each factor's influence and interaction. Processing factors, such as traverse speed, rotation speed and tool tilt angle, are denoted in this Pareto chart as factors  $A$ ,  $B$  and  $C$ , respectively. Fig. 9 shows the pareto chart, which shows that factor  $B$  (traverse speed) has a more significant impact than the other factors and their interactions.

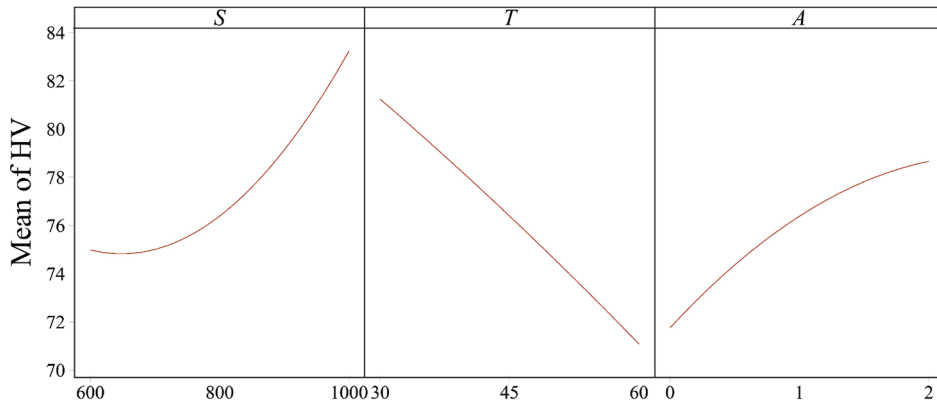


Fig. 7. Mean effects of individual processing factors on hardness

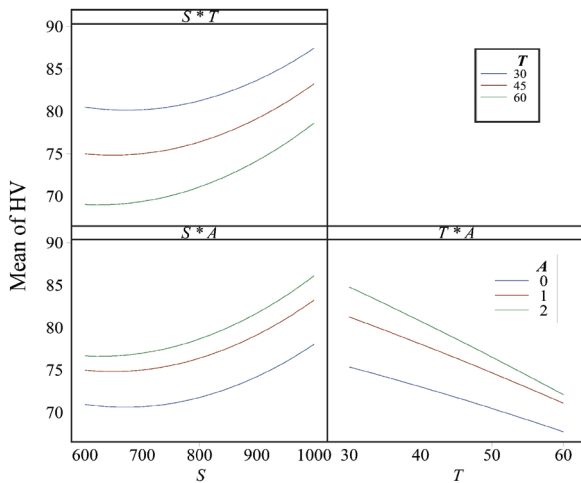


Fig. 8. Interaction plot for Hardness vs. RS, TS, TTA

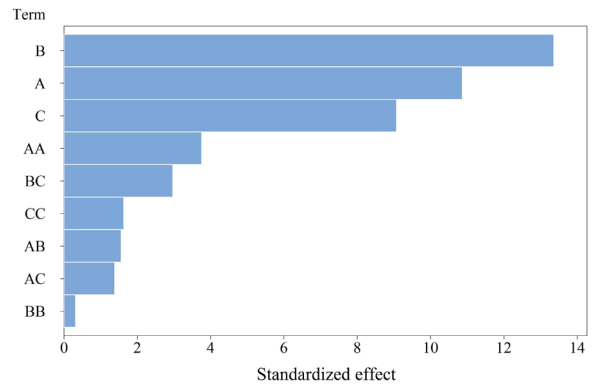


Fig. 9. Pareto chart

desirability diagram is shown in Fig. 10, which shows the maximum hardness is 92 HV with a desirability of 0.98.

#### 4 OPTIMISATION

The statistical techniques used to optimise processes are widespread: overlaying contour plot method, constrained optimisation and desirability approach. The desirability approach is an optimization method that is simple and flexible [15]. The desirability approach is widely used to solve problems with several optimization responses. Desirability is a technique that converts the multiple outputs to measure performance in a set of dimensional quantities. The methodology used in this paper is desirability for optimization of the factor of the FSW process. The FSW processing factor is set in the range: rotational speed from 600 rpm to 1000 rpm, traverse speed (30 mm/min to 60 mm/min) and tool tilt angle (0 deg to 2 deg), and maximize output is set for hardness. From the results, it is observed that the optimum processing factor is  $TTA2$  deg,  $RS1000$  rpm and  $TS30$  mm/min. The

#### 5 VALIDATION OF RESULTS

The confirmatory test was performed with the optimum processing factors. The confirmatory test revealed that FSW Al/Mg Alloys have a hardness of 92.5 HV. The tensile strength of the welded joint is tested with a universal testing machine (UTM), and the specimen is prepared according to ASTM E8. The tensile strength of the welded joint is 182 MPa. The Vicker's hardness of aluminium alloy 6061 is 107 HV and magnesium alloy AZ31B is 83HV. The hardness of FSW is 92 HV, which is 85% Al alloy and 110% Mg alloy, as shown in the graph (Fig. 11).

Masoudian et al. [23] have analysed the effect of process parameters in dissimilarly welded aluminium AA6061 and magnesium AZ31B alloys without tool offset and predicted possible high hardness is around 89 HV. In this research paper, the highest hardness value achieved by tool offset is 92 HV, which is

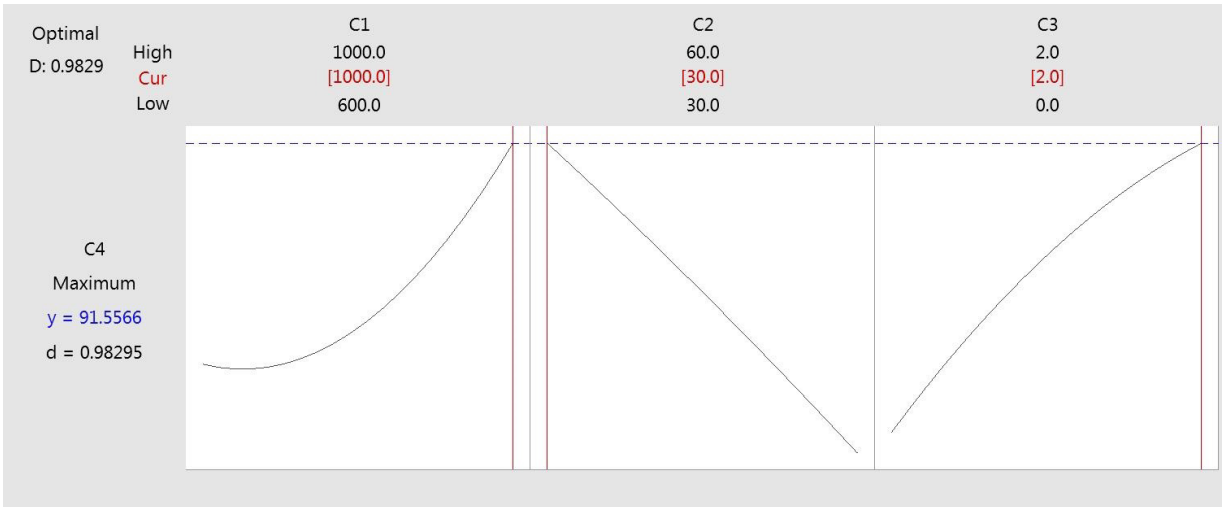


Fig. 10. Desirability diagram



Fig. 11. Vicker's hardness value of base metal and welded specimen

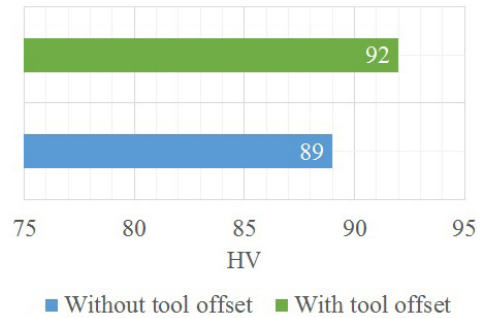


Fig. 12. Vicker's hardness value of with and without tool offset

slightly higher than the experiment done without tool offset as shown in Fig. 12.

Fig. 13 shows the image of an AA 6061-Mg AZ31B joint obtained at 1000 rpm and a 30 mm/min feed rate. Fig. 14 shows the multiple positions used for microstructural investigation after friction stir welding. This investigation provides for a better understanding of friction stir welding behaviour. We selected this condition because the heat generated at the spindle speed of 1000 rpm was sufficient to properly weld and produce the material flush. The aluminium-magnesium weld with a weld-line offset toward aluminium is the subject of this microstructure analysis.

Fig. 14 shows the microstructures generated for the points highlighted. A digital microscope is used to examine the defect-free weld connection. The microstructure of AA6061 and AZ31B's base materials comprises grains of different sizes and distributions.

Recrystallization occurs in Region A, which is referred as to as the nugget zone, as shown in Fig. 14a. Due to the high temperature caused by friction between the tool pin and workpieces, recrystallized Aluminium and Magnesium crystals can be visible in this region. Here the figure shows the aluminium and magnesium crystal distributed evenly.

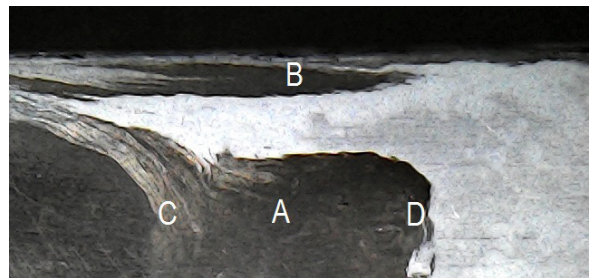
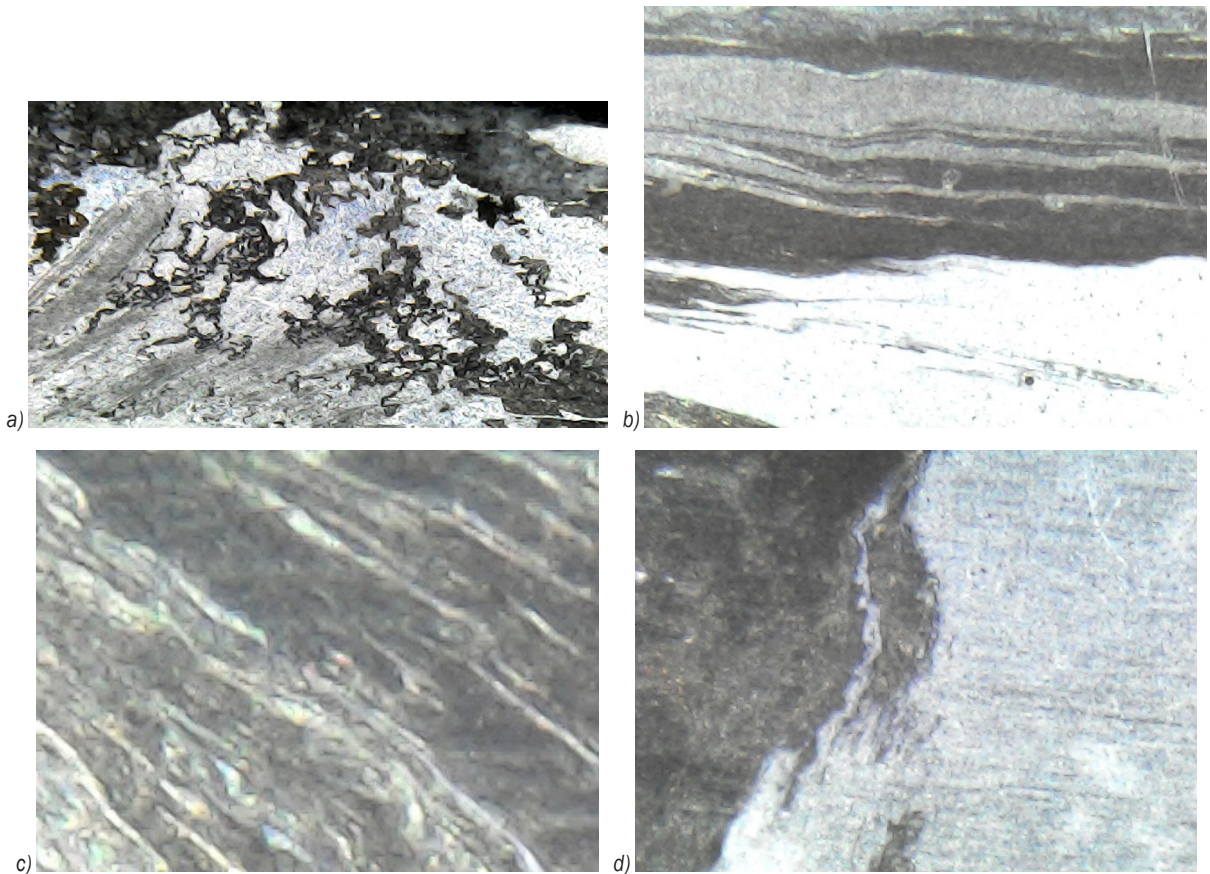


Fig. 13. Friction stir welded AA6061-Mg AZ31B joint and positions of microstructure at the interfacial region

A nugget zone at the shoulder is termed Region B is shown in Fig. 14b. Due to the high temperature



**Fig. 14.** Microstructure at various zones of friction stir welded joint: a) nugget zone, b) nugget region near shoulder, c) thermo-mechanically affected zone in Al AA6061, and d) thermo-mechanically affected zone in Mg AZ31B

caused by friction between the tool shoulder and the workpieces, recrystallized Al and Mg crystals may be visible in this region.

The thermomechanical affected zones of the AA6061 and AZ31B sides are Regions C and D shown in Fig. 14c and d. Due to limited strain deformation, this area exhibits elongated grains and a highly distorted structure. No recrystallization occurred in the region. Only plastic deformation occurs in this region.

## 6 CONCLUSION

The FSW experiment is performed by varying processing factors, and the hardness value of the welded zone was evaluated using the Vicker's hardness tester. The regression equation is established to examine the impact of each factor on the hardness. The adequacy of the regression equation is checked with the help of ANOVA analysis.

The generated model is adequate. The percentages contributed by each factor are  $S = 28.24\%$ ,  $T = 42.72\%$

and  $A = 19.70\%$ , respectively. The traverse and rotational speed have a major impact on the hardness of dissimilar Al/Mg welded joints when compared to the tool tilt angle.

The hardness value of welded joints increases when the RS and TTA increase. The reduction in traverse speed results in high hardness. The traverse speed has a greater effect on the hardness of dissimilarly welded Al/Mg joints than the rotational speed and tilt angle. The optimum processing factor is determined using the desirability approach.

The optimal setting for achieving high hardness (i.e., 92 HV) is at  $S = 1000$  rpm,  $T = 30$  mm/min and  $A = 2$  deg at a desirability value of 0.98. The results of the confirmatory test show that the hardness of FSW Al/Mg alloys is 92.5 HV and tensile strength is 182 MPa.

The hardness of dissimilar FSW Al/Mg alloy is 92 HV, which is 85 % of the hardness of the Al alloy and 110 % of the hardness of the Mg alloy.

## 7 REFERENCE

- [1] Thomas, W.M., Nicholas, E.D. (1997). Friction stir welding for the transportation industries. *Materials and Design*, vol. 18, no. 4-6, p. 269-273, DOI:10.1016/S0261-3069(97)00062-9.
- [2] Mishra, R.S., Ma, Z.Y. (2005). Friction stir welding and processing. *Materials Science and Engineering: R: Reports*, vol. 50, no. 1-2, p. 1-78, DOI:10.1016/j.mser.2005.07.001.
- [3] Nandan, R., DebRoy, T., Bhadeshia, H.K.D.H. (2008). Recent advances in friction-stir welding - Process, weldment structure and properties. *Progress in Materials Science*, vol. 53, no. 6, p. 980-1023, DOI:10.1016/j.pmatsci.2008.05.001.
- [4] Rajakumar, S., Muralidharan, C., Balasubramanian, V. (2011). Predicting tensile strength, hardness and corrosion rate of friction stir welded AA6061-T6 aluminium alloy joints. *Materials and Design*, vol. 32, no. 5, p. 2878-2890, DOI:10.1016/j.matdes.2010.12.025.
- [5] Elangovan, K., Balasubramanian, V. (2008). Influences of tool pin profile and tool shoulder diameter on the formation of friction stir processing zone in AA6061 aluminium alloy. *Materials and Design*, vol. 29 no. 2, p. 362-373, DOI:10.1016/j.matdes.2007.01.030.
- [6] Malarvizhi, S., Balasubramanian, V. (2012). Influences of tool shoulder diameter to plate thickness ratio (D/T) on stir zone formation and tensile properties of friction stir welded dissimilar joints of AA6061 aluminum-AZ31B magnesium alloys. *Materials & Design*, vol. 40, p. 453-460, DOI:10.1016/j.matdes.2012.04.008.
- [7] Sevel, P., Jaiganesh, V. (2015). Effect of tool shoulder diameter to plate thickness ratio on mechanical properties and nugget zone characteristics during FSW of dissimilar Mg alloys. *Transactions of the Indian Institute of Metals*, vol. 68, no. 1, p. 41-46, DOI:10.1007/s12666-015-0602-0.
- [8] Verma, J., Taiwade, R.V., Reddy, C., Khatirkar, R.K. (2018). Effect of friction stir welding process parameters on Mg-AZ31B/Al-AA6061 joints. *Materials and Manufacturing Processes*, vol. 33, no. 3, p. 308-314, DOI:10.1080/10426914.2017.1291957.
- [9] Li, W.Y., Fu, T., Hütsch, L., Hilgert, J., Wang, F.F., dos Santos, J.F., Huber, N. (2014). Effects of tool rotational and welding speed on microstructure and mechanical properties of bobbin-tool friction-stir welded Mg AZ31. *Materials and Design*, vol. 64, p. 714-720, DOI:10.1016/j.matdes.2014.07.023.
- [10] Singh, K., Singh, G., Singh, H. (2018). Investigation of microstructure and mechanical properties of friction stir welded AZ61 magnesium alloy joint. *Journal of Magnesium and Alloys*, vol. 6, no. 3, p. 292-298, DOI:10.1016/j.jma.2018.05.004.
- [11] Devaiah, D., Kishore, K., Laxminarayana, P. (2018). Optimal FSW process parameters for dissimilar aluminium alloys (AA5083 and AA6061) using Taguchi Technique. *Materials Today: Proceedings*, vol. 5, no. 2, p. 4607-4614, DOI:10.1016/j.matpr.2017.12.031.
- [12] Wang, W., Deng, D., Mao, Z., Tong, Y., Ran, Y. (2017). Influence of tool rotation rates on temperature profiles and mechanical properties of friction stir welded AZ31 magnesium alloy. *International Journal of Advanced Manufacturing Technology*, vol. 88, p. 2191-2200, DOI:10.1007/s00170-016-8918-4.
- [13] Barla, M., Jaidi, J. (2018). Influence of strain hardening behaviour in friction stir welded joints of aluminium-alloy plates. *Materials Today: Proceedings*, vol 5, no. 2, p. 3851-3860, DOI:10.1016/j.matpr.2017.11.639.
- [14] Sahu; P.K., Pal, S., Pal, S.K., Jain, R. (2016). Influence of plate position, tool offset and tool rotational speed on mechanical properties and microstructures of dissimilar Al/Cu friction stir welding joints. *Journal of Materials Processing Technology*, vol. 235, p. 55-67, DOI:10.1016/j.jmatprotec.2016.04.014.
- [15] Elatharasan, G., Senthil Kumar, V.S. (2012). Modelling and optimization of friction stir welding parameters for dissimilar aluminium alloys using RSM. *Procedia Engineering*, vol. 38, p. 3477-3481, DOI:10.1016/j.proeng.2012.06.401.
- [16] Elatharasan, G., Senthil Kumar, V.S. (2014). Corrosion analysis of friction stir-welded AA 7075 aluminium alloy. *Strojniški vestnik - Journal of Mechanical Engineering*, vol. 60, no. 1, p. 29-34, DOI:10.5545/sv-jme.2012.711.
- [17] Bucki, T., Konieczny, M., Bolibruchova, D., Rzepa, S. (2021). Characterization of the AZ31/AW-6060 joint fabricated using compound casting with a Zn interlayer at relatively low-temperature conditions. *Strojniški vestnik - Journal of Mechanical Engineering*, vol. 67, no. 7-8, p. 389-397, DOI:10.5545/sv-jme.2021.7262.
- [18] Li, G., Jiang, W., Guan, F., Zhu, J., Zhang, Z., Fan, Z. (2020). Microstructure, mechanical properties and corrosion resistance of A356 aluminum/AZ91D magnesium bimetal prepared by a compound casting combined with a novel Ni-Cu composite interlayer. *Journal of Materials Processing Technology*, vol. 288, art. ID 116874, DOI:10.1016/j.jmatprotec.2020.116874.
- [19] Li, G., Jiang, W., Yang, W., Jiang, Z., Guan, H., Jin, H., Fan, Z. (2019). New insights into the characterization and formation of the interface of A356/AZ91D bimetallic composites fabricated by compound casting. *Metallurgical and Materials Transactions A*, vol. 50, p. 1076-1090, DOI:10.1007/s11661-018-5022-44.
- [20] Vasantha Kumar, K.P., Balasubramanian, M. (2020). Analyzing the effect of FSW process parameter on mechanical properties for a dissimilar aluminium AA6061 and magnesium AZ31B alloy. *Materials Today: Proceedings*, vol. 22, p. 2883-2889, DOI:10.1016/j.matpr.2020.03.421.
- [21] Karthikeyan, R., Balasubramanian, V. (2010). Predictions of the optimized friction stir spot welding process parameters for joining AA2024 aluminum alloy using RSM. *International Journal of Advanced Manufacturing Technology*, vol. 51, p. 173-183, DOI:10.1007/s00170-010-2618-2.
- [22] Palanivel, R., Koshy Mathews, P. (2012). Prediction and optimization of process parameter of friction stir welded AA5083-H111 aluminum alloy using response surface methodology. *Journal of Central South University*, vol. 19, p. 1-8, DOI:10.1007/s11771-012-0964-y.
- [23] Masoudian, A., Tahaei, A., Shakiba, A., Sharifianjazi, F., Mohandes, J.A. (2014). Microstructure and mechanical properties of friction stir weld of dissimilar AZ31-O magnesium alloy to 6061-T6 aluminum alloy. *Transactions of Non-ferrous Metals Society of China*, vol. 24, no. 5, p. 1317-1322, DOI:10.1016/S1003-6326(14)63194-0.